Psychological distress in men with prostate cancer receiving adjuvant androgen-deprivation therapy.

CHEMISTRY
A EUROPEAN JOURNAL

Supporting Information

The Effect of Hydrosilanes on the Active Sites of the Phillips Catalyst: The Secret for In Situ α-Olefin Generation

Caterina Barzan,[a] Diego Gianolio,[b] Elena Groppo,*[a] Carlo Lamberti,[a] Vincent Monteil,[c] Elsje Alessandra Quadrelli,*[c] and Silvia Bordiga[a]

chem_201303156_sm_miscellaneous_information.pdf

Supplementary Information

S1. Experimental: additional details

Samples preparation and reactivity

$Cr(II)/SiO_2$ samples were prepared following the procedure discussed in the main text, as reported previously.[1] Modification of the $Cr(II)/SiO_2$ samples, $\mathbf{Cr_{PHL}}$, was achieved by using two different hydrosilane molecules, SiH_4 and triethylsilane (TES), leading to $\mathbf{Cr_{SiH4}}$ and $\mathbf{Cr_{TES}}$, respectively. The former was dosed from the gas phase diluted in Ar at 5000 ppm; whereas TES (which is liquid at room temperature) was dosed from the vapor phase. Ethylene polymerization was performed at room temperature in the gas phase at an equilibrium pressure in the range of 100 - 300 mbar, inside the same cell used for spectroscopic measurements.

Techniques

FT-IR spectroscopy

Transmission FT-IR spectra were collected in the 4500 – 800 cm^{-1} range at 2 cm^{-1} resolution on a Bruker Vertex70 instrument equipped with a MCT detector. The samples, in the form of thin self-supported wafers (surface density ca. 10 mg cm^{-2}), were placed inside a home-made IR cells equipped with KBr windows and designed to perform thermal treatments in the 1000–77 K range. The activation was performed directly into the IR cell where FT-IR experiments were conducted, thus avoiding any catalyst poisoning.

Diffuse Reflectance UV-Vis spectroscopy

Diffuse Reflectance UV-Vis spectra were recorded on a Varian Cary5000 instrument equipped with a reflectance sphere. The sample, in the form of a thick self-supported pellet (surface density ca. 60 mg cm^{-2}), was placed inside a home-made quartz cell equipped with a window in optical quartz (suprasil), allowing to perform thermal treatments in the 1000 – 300 K range, both in vacuum and in presence of gas. As for FT-IR measurements, the sample activation was performed in the same cell used for UV-Vis measurements.

X-ray absorption spectroscopy (XAS)

X-ray absorption experiments at the Cr K-edge (5989 eV) were performed at the BM01B beamline of the Swiss-Norwegian beamlines (SNBL) of the European Synchrotron Radiation Facility (ESRF, Grenoble, F). The white beam was monochromatized using a Si(111) double crystal. Harmonic rejection was performed by detuning. Due to Cr dilution, EXAFS spectra were collected in fluorescence mode, by means of a 13 elements Ge detector with fast digital multi channel analyzer electronics elements. The intensity of the incident beam was monitored by an ionization chamber filled with 1 bar of 20% N_2 – 80% He. The beam transmitted through the sample passed further through a second ionization chamber, a Cr foil and a third ionization chamber to ensure the correct energy calibration for any acquisition.

Due to the high air sensitivity, the samples were measured inside sealed capillaries (1.0 mm in diameter), following the well established procedure adopted for XRPD experiments. For this reason, the beam was shaped with the vertical slits in order to reach a dimension on the sample of 0.3 mm. For each sample, the horizontal slits were optimized to fit with the interval of uniform filling of the capillary. Sample homogeneity was checked with an X-ray camera.

The same experimental geometry was already applied successfully in the characterization of the $\mathbf{Cr_{PHL}}$ catalyst.[2]

The XANES part of the spectra was acquired with an energy step of 0.4 eV and an integration time of 2s/point. The EXAFS part of the spectra was collected up to 12 $Å^{-1}$ with a variable sampling step in energy, resulting in $\Delta k = 0.05$ $Å^{-1}$, and an integration time that linearly increases as a function of k from 5 to 20 s/point to account for the low signal-to-noise ratio at high k values. For each sample, three equivalent EXAFS spectra were acquired and averaged before the data analysis.

Polyethylene characterization: DSC and SEC

Melting temperatures and molecular weight distributions of the polyethylenes resulting from ethylene polymerization on the $\mathbf{Cr_{PHL}}$, $\mathbf{Cr_{TES}}$ and $\mathbf{Cr_{SiH4}}$ catalysts were obtained with differential scanning calorimetry (DSC) and size exclusion chromatography (SEC), respectively. Differential scanning calorimetry (DSC) was performed on a Mettler Toledo DSC1 at a heating rate of 10 °C min^{-1}. Two successive heating and cooling of the samples were performed. Melting point (T_m) values were obtained during the second heating cycle. SEC measurements were performed on a Waters Alliance GPCV 2000 instrument equipped with two detectors (viscosimeter and refractometer). SEC analysis was performed at 150 °C in 1,2,4-trichlorobenzene at a flow rate of 1 mL min^{-1}.

S2. Monitoring ethylene polymerization over Cr_{TES} and Cr_{SiH4} catalysts by means of in-situ FT-IR spectroscopy.

FT-IR spectroscopy was applied to follow in situ ethylene polymerization at room temperature on both $\mathbf{Cr_{TES}}$ and $\mathbf{Cr_{SiH4}}$ catalysts. Figure S1 shows the FT-IR spectra collected within the first eight minutes of ethylene polymerization at room temperature on the two catalysts, in the $\nu(CH_x)$ (parts a and c) and in the $\delta(CH_x)$ (parts b and d) regions, respectively. The spectra were recorded at a time resolution of 8 s and at constant ethylene pressure (200 mbar). Note that for $\mathbf{Cr_{TES}}$ the IR spectra collected during ethylene polymerization have been subtracted to the spectrum of the sample prior ethylene admission in the cell, in order to remove the contribution of the alkyl groups remaining on the sample (see Figure 1a in the main text). The two sequences of spectra collected during ethylene polymerization on $\mathbf{Cr_{TES}}$ and $\mathbf{Cr_{SiH4}}$ catalysts are very similar. Four IR absorption bands are observed in the 3000-2800 cm^{-1} region (Figure S1a,c): i) the IR bands at 2920 and 2851 cm^{-1} are assigned to the asymmetric and symmetric $\nu(CH_2)$ modes; whereas ii) the IR bands at 2965 and 2877 cm^{-1} are assigned to the asymmetric and symmetric stretching modes of CH_3 groups, respectively. The latter band is rapidly hidden by the more intense IR absorption bands due to CH_2 species. The corresponding $\delta(CH_2)$ and $\delta(CH_3)$ absorption bands occur at 1472, 1463 and 1379 cm^{-1}, respectively (Figure S1b,d).

For both $\mathbf{Cr_{SiH4}}$ and $\mathbf{Cr_{TES}}$ catalysts the observation of IR absorption bands characteristic of methyl groups demonstrates that the formed polyethylene contains more CH_3 moieties than that formed on $\mathbf{Cr_{PHL}}$ (which yields long polyethylene chains without branches, HDPE), indicating either higher branching and/or shorter CH_3-terminated chains.

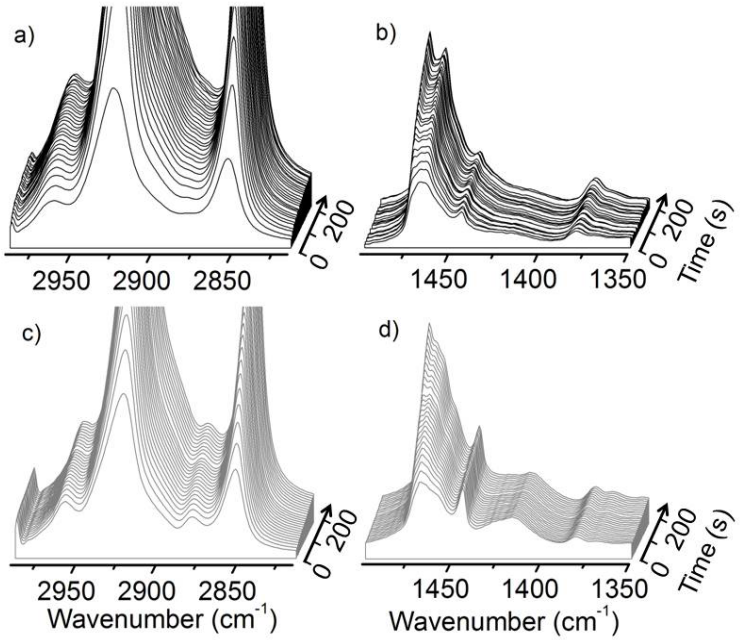

Figure S1. Ethylene polymerization at room temperature on $\mathbf{Cr_{SiH4}}$ (black) and $\mathbf{Cr_{TES}}$ (grey) catalysts followed in situ by FT-IR spectroscopy. The FT-IR spectra, collected within the first eight minutes of reaction, are shown in the $\nu(CH_x)$ (parts a and c) and $\delta(CH_x)$ (parts b and d) regions, respectively.

S3. Main properties of the polyethylene products: DSC and SEC analysis

Figure S2a shows the DSC curves of the polyethylenes that were recovered after ethylene polymerization followed by in-situ FT-IR spectroscopy on $\mathbf{Cr_{PHL}}$, $\mathbf{Cr_{SiH4}}$ and $\mathbf{Cr_{TES}}$. Figure S2b shows the corresponding MW distributions. The same data are summarized in Table 1 in the main text.

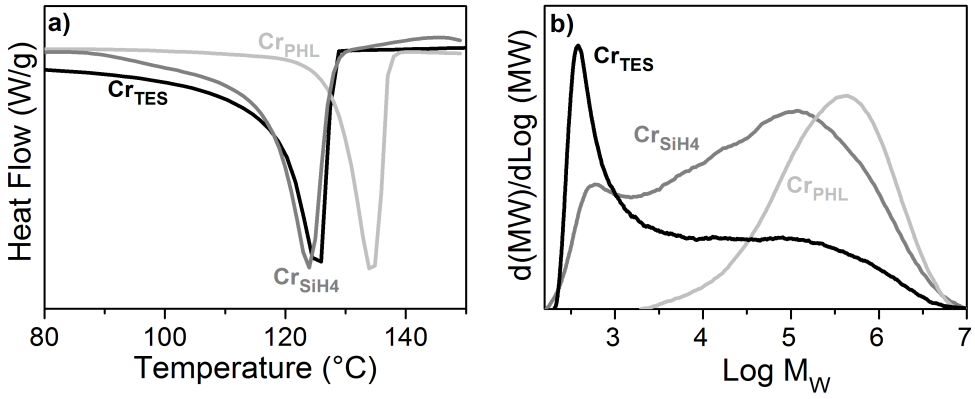

Figure S2. DSC signals (part a) and molecular weight distributions from size exclusion chromatography (part b) of the polymers produced with the $\mathbf{Cr_{PHL}}$ (light grey), and with the same catalyst after modification with SiH_4 (grey) and TES (black).

The MW distribution of the polymer made with the $\mathbf{Cr_{PHL}}$ catalyst is broad (M_w = 600000 $gmol^{-1}$, dispersity $Đ = M_w / M_n = 7.0$), as usually found for a polyethylene synthesized with a multi-site Phillips catalyst. The corresponding DSC curve shows a melting peak at 134 °C characteristic of HDPE having a negligible level of branching, classically obtained with a Phillips catalyst.

On the contrary, the solid product obtained with the $\mathbf{Cr_{SiH4}}$ and $\mathbf{Cr_{TES}}$ catalysts is characterized by a bimodal molecular weight distribution, composed of two main components: a heavier one, in the same molecular weight range to the polyethylene obtained with $\mathbf{Cr_{PHL}}$ catalyst (more precisely the molecular weight of this heavier component is slightly lower and broader than that observed with $\mathbf{Cr_{PHL}}$ catalyst), and a very low MW fraction centered at about $M_p = 10^3$ g/mol. For $\mathbf{Cr_{TES}}$ this latter fraction of ethylene products is even more pronounced. In both cases the resulting polymers melt at a much lower temperature (123-125°C), which is characteristic of a polyethylene with a higher level of branching (such as LLDPE). A similar T_m is observed for LLDPE obtained by copolymerization of ethylene and α-olefins.[3]

S4. FT-IR spectra of adsorbed CO at room temperature: comparison between a ^{12}CO:^{13}CO mixture (1:1 ratio), pure ^{12}CO and pure ^{13}CO.

As discussed in the main text, the IR spectrum of CO adsorbed at room temperature on $\mathbf{Cr_{TES}}$ catalyst (black in Figure S3) is dominated by an intense absorption band at 1990 cm^{-1} and by a weaker band at 2024 cm^{-1}, which can be tentatively assigned to the ν_{asym} and ν_{sym} vibrational modes of a chromium dicarbonyl species. The weakness of the absorption band ascribed to dicarbonyl ν_{sym}, suggests a wide angle between the two CO moieties.[4-6] When ^{13}CO is used instead of ^{12}CO (light grey in Figure S3), the two absorption bands are isotopically red-shifted by the theoretical 0.9777 factor based on the Hooke law ($\nu(^{13}CO)$ = 1945 and 1975 cm^{-1}); a weak absorption band at 1913 cm^{-1} is also present and assigned to $^{12}C^{18}O$ traces in the ^{13}CO feed.

IR spectra of CO isotopic mixtures is a widely employed technique for the assignment of complex IR carbonyl bands.[7] The IR spectrum of $\mathbf{Cr_{TES}}$ after addition of a 1:1 mixture of ^{12}CO and ^{13}CO isotopic isomers (dark grey in Figure S3) can be deconvoluted in terms of 6 components: i) the two doublets already observed for carbonyl species of pure ^{12}CO and pure ^{13}CO (2024-1990 cm^{-1} and 1975-1945 cm^{-1}, respectively); and ii) two singlets at 2009 and 1960 cm^{-1}. These two singlets fall exactly in the baricenter of the two aforementioned doublets. This IR absorption pattern is typical of dicarbonyl species; in fact, besides the two doublets due to pure $(^{12}CO)_2$ and pure $(^{13}CO)_2$ dicarbonyls, the mixed $(^{12}CO)(^{13}CO)$ species behave as two de-coupled mono-carbonyls. These data provide strong evidence that dicarbonyl species are formed upon dosage of CO on $\mathbf{Cr_{TES}}$.

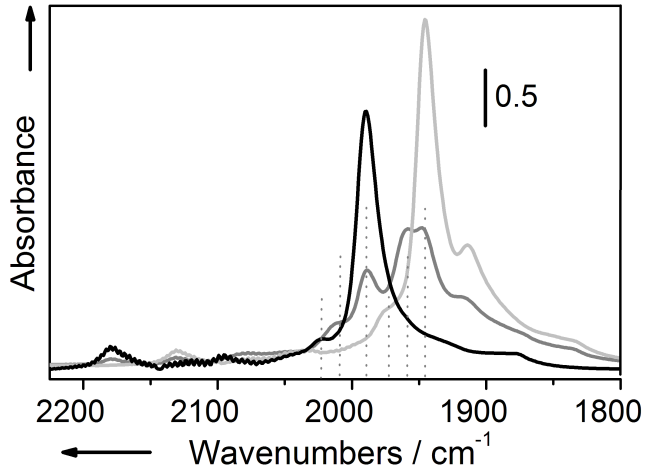

Figure S3. IR spectra of $\mathbf{Cr_{TES}}$ in interaction with: i) ^{12}CO (black); ii) ^{13}CO (light grey); and iii) a mixture of ^{12}CO:^{13}CO = 1:1 (dark grey). All spectra are recorded at room temperature.

S5. Electronic properties of $\mathbf{Cr_{TES}}$ in presence of CO

Both diffuse reflectance UV-Vis and XANES spectra greatly change when the $\mathbf{Cr_{TES}}$ catalyst is contacted with CO (light grey spectra in Figure S4) and reveal the formation of "classical" carbonyls, in agreement with FT-IR results. In the DR UV-Vis spectrum (Figure S4a), the d-d bands shift towards higher wavenumbers when CO molecule interacts with the modified chromium sites, as expected upon increasing the ligand field around the chromium sites. Even more important is the change occurring in the charge-transfer region: the characteristic band around 30000 cm^{-1} due to O → Cr(II) charge-transfer shifts at higher wavenumbers (31800 cm^{-1}), accompanied by the appearance of two intense bands at 36500 and 43200 cm^{-1}. Similar intense bands in the ultraviolet region have been observed in the UV-Vis spectra of homogeneous Cr carbonyl complexes, and assigned to electronic transitions from a Cr(d) full orbital, to the empty CO 2π* orbital.[8]

In the XANES spectrum (Figure S4b), interaction of CO at room temperature with $\mathbf{Cr_{TES}}$ causes the appearance of two well-defined components on the edge, around 6005 and 6020 eV, typical of metal carbonyl complexes and due to transitions from Cr(1s) to CO 2π* orbitals.[9-11] Similar features were already observed in the spectrum of $\mathbf{Cr_{PHL}}$ in interaction with CO at 100 K,[2] *i.e.* in presence of chromium carbonyls having a "classical" behavior. The intensity of these two components in the present spectrum is slightly lower than for carbonyls formed on $\mathbf{Cr_{PHL}}$ at 100 K, in agreement with the formation of dicarbonyl species (as suggested by FT-IR spectroscopy and demonstrated in the following by EXAFS data analysis).

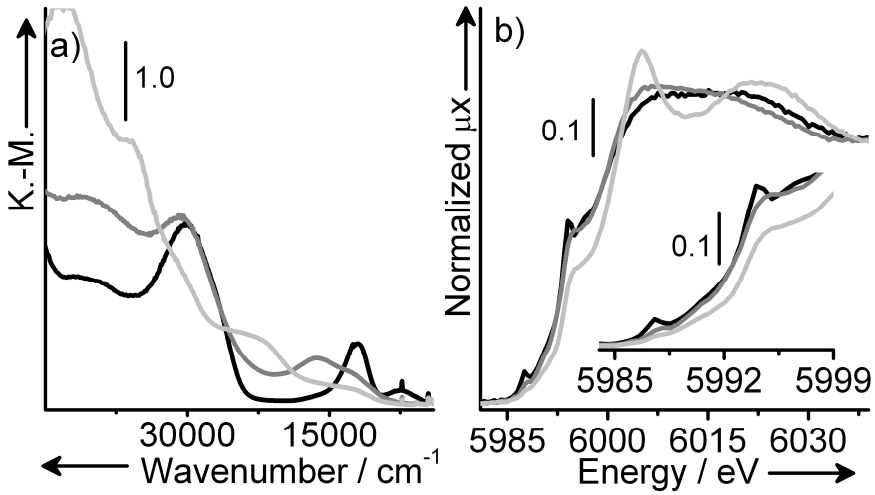

Figure S4. DR UV-Vis (part a) and XANES (part b) spectra of $\mathbf{Cr_{PHL}}$ (black), $\mathbf{Cr_{TES}}$ (grey) and of $\mathbf{Cr_{TES}}$ after interaction with CO at room temperature (light grey). Inset in part b) shows a magnification of the pre-edge region.

S6. XANES simulations of $\mathbf{Cr_{PHL}}$ and $\mathbf{Cr_{TES}}$ catalysts.

XANES simulations on $\mathbf{Cr_{PHL}}$ and $\mathbf{Cr_{TES}}$ catalysts were performed using FEFF8.4 code.[12] Two spherical clusters centred on the Cr absorbing atom and with radius of 5Å obtained starting from the possible structures shown in Scheme 1 (part 1) and c) in main text and Table S1) were used as input geometries. Hedin-Lunqvist exchange correlation potential has been adopted for the calculations leaving the imaginary part equal to zero; core hole effects were included. The simulated curves are able to reproduce the two pre-edge features both in terms of relative intensities and energy positions. The intensity of the white line is slightly underestimated and the features after the edge are slightly shifted probably due to the fact that the input geometries do not include the second shell siloxane groups (see Scheme 2 in the

main text). On the basis of the calculated projected density of states both features are assigned to transitions from Cr(1s) to valence levels characterized by significant p/d hybridization.
When the experimental $\mathbf{Cr_{TES}}$ spectrum is compared to the $\mathbf{Cr_{PHL}}$ a shift toward lower energies and increase of intensity of the white line are observed. Both features are well reproduced by the simulations adopting a longer Cr-O first shell distance in agreement with the data obtained by EXAFS fit. The longer Cr-O distance is also responsible for the decrease of the pre-edge features intensity because of the reduced overlap between O(2p) and Cr(3d) orbitals.

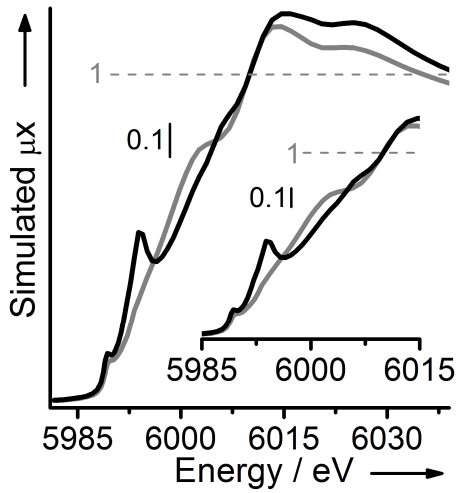

Figure S5. XANES simulated spectra of $\mathbf{Cr_{PHL}}$ (black) and $\mathbf{Cr_{TES}}$ (grey) calculated by FEFF8.4. Inset shows a magnification of the pre-edge region.

S7. EXAFS data analysis

Figure S6a shows the k^3-weighted $\chi(k)$ functions of the $\mathbf{Cr_{PHL}}$ (black) and $\mathbf{Cr_{TES}}$ (grey) catalysts, as already reported in the main text, and the spectrum of $\mathbf{Cr_{TES}}$ in interaction with CO (light grey). Figure S6b shows the corresponding FT, in both modulus and imaginary parts (top and bottom, respectively). All the k^3-weighted $\chi(k)$ functions were Fourier Transformed in the Δk = 2.0-10.0 $Å^{-1}$ range. At higher k values the noise becomes quite high: this is due to the fact that the data were collected in fluorescence mode on highly diluted samples, in an unfavorable geometrical configuration (sample in sealed capillary, requiring incoming X-rays and florescence X-rays to cross twice the absorbing SiO_2 container). For this reason we decided to perform the FT in a safe, but short k-range.

EXAFS data analysis was performed using the Arthemis software.[13] Phase and amplitudes were calculated by FEFF6.0 code[14] using as input the simple Cr-O, Cr-Si and Cr-CO fragments, the latter assumed to be linear. The validity of the FEFF6.0 code to compute correctly phases and amplitudes for Cr^{II}-(light scatterers) has been successfully verified with Cp_2Cr in toluene solution.[15] For each sample, the averaged $k^3\chi(k)$ function was Fourier transformed (FT) in the Δk = 2.0-10.0 $Å^{-1}$ interval so that a direct comparison among the different fits can be done. The fits were performed in different R-spaces as detailed for each specific case, by respecting the Nyquist theorem (number of independent points < $2\Delta k\Delta R/\pi$) in its more strict form.[16,17]

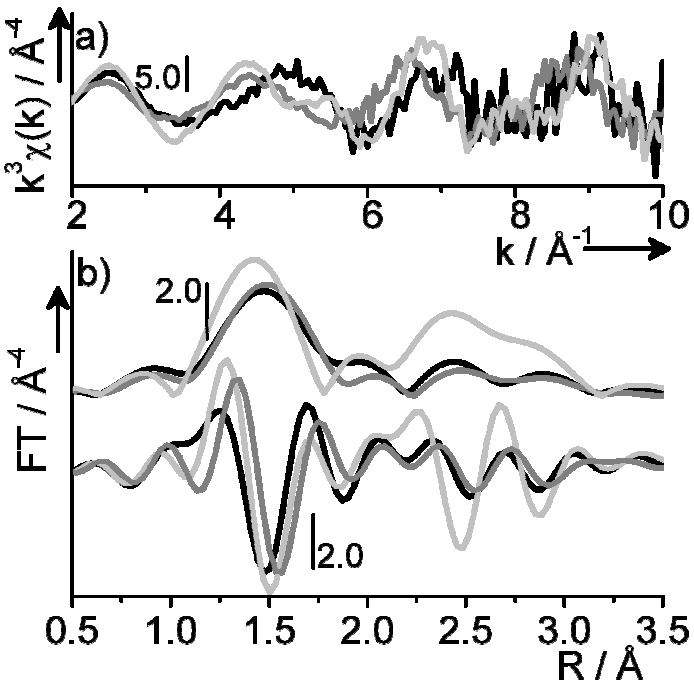

Figure S6. k^3-weighted $\chi(k)$ functions (part a) and corresponding FT (in both modulus and imaginary parts, part b) performed in the Δk = 2-10 Å^{-1} range for $\mathbf{Cr_{PHL}}$ (black), $\mathbf{Cr_{TES}}$ (dark grey) catalyst, and the same after interaction with CO at room temperature (light grey).

$\mathbf{Cr_{TES}}$: a first shell analysis

As already discussed in the main text, the FT spectrum of $\mathbf{Cr_{PHL}}$ is dominated by a first shell signal at 1.47 Å (not corrected in phase); additional contributions are present around 2.7 Å. This spectrum well reproduces the one reported in our previous work. The results of the analysis discussed previously are summarized in Table S1. In average, the first coordination sphere around Cr(II) sites is composed of two oxygen ligands at a distance of about 1.86 ± 0.03 Å, having a σ^2 value of 0.015 ± 0.005A Å^2: the Debye-Waller factor is in agreement with the expected heterogeneity of the grafted Cr(II) sites. The contributions at longer distance were attributed to both, silicon atoms in the second coordination shell and oxygen atoms belonging to weaker siloxane ligands.

The first shell contribution clearly shifts at longer distance in $\mathbf{Cr_{TES}}$, suggesting that, in average, the first shell ligands are at longer distance. In the analysis of the EXAFS spectrum, we used as input models the three schematic structures shown in Scheme 1 in the main text, in which the chromium absorbing atom is surrounded by one oxygen (and one hydrogen, not detectable by EXAFS) in model a), one oxygen and one silicon in model b), and two independent oxygen atoms in model c). In all the cases it was found that the coordination number and the Debye-Waller factors of the different contributions strongly correlate each others. Therefore, we decided to fix in all the three cases the number of the first shell neighbors, and to optimize all the other parameters. Table S1 summarizes the results obtained by adopting the same fitting strategy with the three different models, compared to the results of the fit performed previously on $\mathbf{Cr_{PHL}}$ sample. It is clear that only model c) gives a satisfactory fit, whereas both models a) and b) give non-physical values (asterisks in the Table S1). The quality of the fit for model c) is shown in Figure S6.

As discussed in the main text, EXAFS analysis demonstrates that, in average the modified chromium sites are still coordinated to two oxygen atoms, at a distance longer than those present in the $\mathbf{Cr_{PHL}}$ sample. The low value of $\sigma^2_{Cr\text{-}O}$ is in good agreement with the

homogeneous nature of the modified chromium sites, as determined by FT-IR spectroscopy of adsorbed CO.

Table S1 - Summary of the optimized parameters in the analysis of EXAFS data for $\mathbf{Cr_{TES}}$ system. Non optimized parameters can be distinguished by the absence of the corresponding error bar. The fits were performed starting by three different models, in the R space (ΔR = 1.1 – 2.5 Å, Δk = 2.0 - 10.0 $Å^{-1}$). For comparison, the second column reports the optimized parameters in the analysis of EXAFS signal for $\mathbf{Cr_{PHL}}$ as obtained previously.[2] Asterisks indicate non physical values obtained from the fit.

	$\mathbf{Cr_{PHL}}$	$\mathbf{Cr_{TES}}$		
		Model a)	Model b)	Model c)
	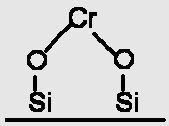	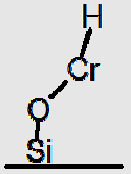	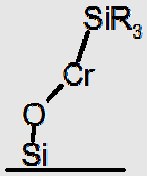	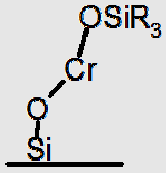
ΔE_0 (eV)	-1 ± 4	-51 ± 25 *	-6 ± 9	-2 ± 6
$S_0^2 x\ N_{Cr-O}$	1.8 ± 0.6	1	1	2
d_{Cr-O} (Å)	1.86 ± 0.03	2.16 ± 0.08	1.8 ± 0.1	1.95 ± 0.03
σ^2_{Cr-O} ($Å^2$)	0.015 ± 0.005	-0.005 ± 0.002 *	-0.0003 ± 0.03 *	0.004 ± 0.002
$S_0^2 x\ N_{Cr-Si}$			1	
d_{Cr-Si} (Å)			-0.002 ± 0.04	
σ^2_{Cr-Si} ($Å^2$)			0.0004 ± 0.02 *	
N_{var} / N_{ind}	4 / 6	3 / 7	5 / 7	3 / 7
R_{factor}	0.031	0.11	0.028	0.10

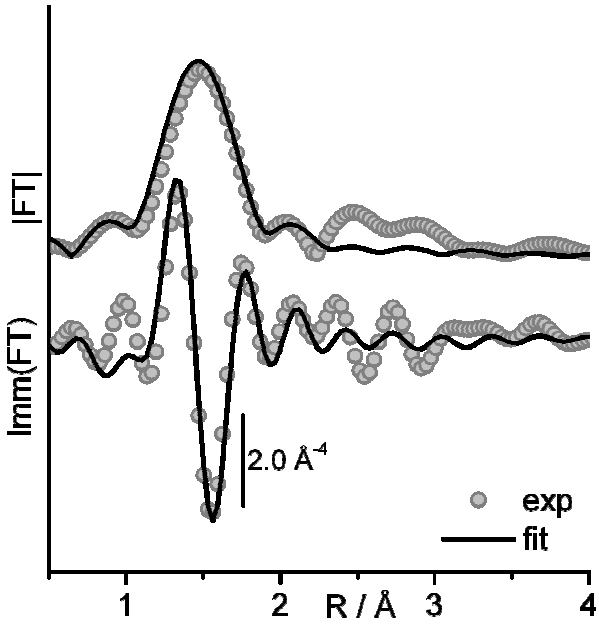

Figure S7. Experimental (dots) and simulated (full line) FT of the k^3-weighted $\chi(k)$ functions for $\mathbf{Cr_{TES}}$, in both modulus (top) and imaginary parts (bottom).

Cr$_{TES}$ + *CO*

When CO is dosed on the $\mathbf{Cr_{TES}}$, the FT of the EXAFS spectrum undergoes relevant changes: i) the first shell signal increases in intensity and shifts back towards shorter distances; ii) at

longer distance, an intense signal appears, which is easily assigned to the multiple scattering contribution of adsorbed CO molecules.[2,10,11]

An additional contribution to the EXAFS signal needs to be considered in the data analysis (Cr–CO paths); this implies that three more variables must be fitted ($N_{Cr–CO}$, $\sigma^2_{Cr–CO}$, $d_{Cr–CO}$), in addition to those needed to describe $\mathbf{Cr_{TES}}$. The high number of variables and, in addition, the high correlation between the fitting parameters, obliged us to perform the analysis in two separate steps. At first, we simulated the experimental signal in the 1.8 – 3.2 Å region, *i.e.* in a R region where the spectrum is dominated by the multiple scattering contribution of the CO ligands. The results of this first fit are summarized in the third column of Table S2. The fit is stable; most of the signal in the 1.8 – 3.2 Å region is well simulated with the multiple scattering contributions of the CO ligands. According to the fit, around two CO molecules are, in average, coordinated to the Cr sites, at a distance of d_{Cr-CO} = 1.981 ± 0.009 Å and having a σ^2_{Cr-CO} = 0.004 ± 0.003 Å^2. The d_{Cr-CO} distance is in good agreement with the value reported by Gianolio et al.[2] on the $\mathbf{Cr_{PHL}}$ sample (1.995 ± 0.008 Å). The average number of carbonyl ligands is in good agreement with that expected from FT-IR data; and the low value of the corresponding Debye-Waller factor confirms that the chromium carbonyl complexes are very homogeneous from a structural point of view. However, it should be noticed that equally good simulations can be obtained by fixing σ^2_{Cr-CO} to slightly higher values; a small increase in the Debye-Waller values is compensated by a small increase in the $N_{Cr–CO}$ value. Due to the high correlation among the fitted variables for an experimental data-set analyzable uo to k = 10 Å^{-1} only, the conclusion is that, upon exposure of $\mathbf{Cr_{TES}}$ to CO, the number of adsorbed CO molecules per chromium is around two, although three can not be excluded.

In a second step of the analysis, the fit was performed in an extended R range (1.1 – 3.2 Å). The variables associated with the carbonyl ligands were fixed to the best values determined in the previous step of the analysis. It was found that it is not possible to fit simultaneously $N_{Cr–O}$ and $\sigma^2_{Cr–O}$, because they are strongly correlated and non physical values are obtained. Therefore, $N_{Cr–O}$ was fixed at 2 (which is reasonable, since formation of carbonyls should not cause any breaking of the Cr-O bonds). The results are summarized in the last column of Table S2, and the quality of the fit is shown in Figure S5.

Table S2 - Summary of the optimized parameters in the analysis of EXAFS data for the $\mathbf{Cr_{TES}}$ and for the same catalyst in interaction with CO at room temperature. Non optimized parameters can be distinguished by the absence of the corresponding error bar. The fits were performed starting in different R spaces, as indicated.

	$\mathbf{Cr_{TES}}$	$\mathbf{Cr_{TES}}$ + CO	
ΔR (Å)	1.1 – 2.5	1.8 – 3.2	1.1 – 3.2
N_{var} / N_{ind}	3 / 7	4 / 7	2 / 10
ΔE_0 (eV)	-2 ± 6	-5 ± 3	-5
$S_0^2 x\ N_{Cr-O}$	2	-	2
d_{Cr-O} (Å)	1.95 ± 0.03	-	1.87 ± 0.01
σ^2_{Cr-O} (Å^2)	0.004 ± 0.002	-	0.011 ± 0.004
$S_0^2 x\ N_{Cr-CO}$	-	1.8 ± 0.6	1.8
d_{Cr-CO} (Å)	-	1.981 ± 0.009	1.981
σ^2_{Cr-CO} (Å^2)	-	0.004 ± 0.003	0.004
R_{factor}	0.086	0.051	0.069

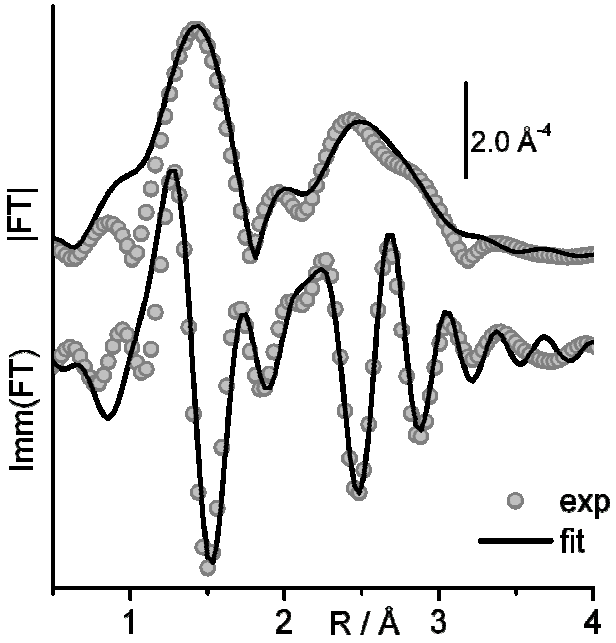

Figure S8. Experimental (dots) and simulated (full line) FT of the k^3-weighted $\chi(k)$ functions for $\mathbf{Cr_{TES}}$ and in interaction with CO at room temperature, in both modulus (top) and imaginary parts (bottom).

References

[1] E. Groppo, C. Lamberti, S. Bordiga, G. Spoto, A. Zecchina, *Chem. Rev.* **2005**, *105*, 115-183.
[2] D. Gianolio, E. Groppo, J. G. Vitillo, A. Damin, S. Bordiga, A. Zecchina, C. Lamberti, *Chem. Commun.* **2010**, *46*, 976–978.
[3] M. P. McDaniel, *Adv. Catal.* **2010**, *53*, 123-606.
[4] H. C. L. Abbenhuis, M. L. W. Vorstenbosch, R. A. van Santen, W. J. J. Smeets, A. L. Spek, *Inorg. Chem.* **1997**, *36*, 6431-6433.
[5] J. J. Rack, J. D. Webb, S. H. Strauss, *Inorg. Chem.* **1996**, *35*, 277-&.
[6] C. Lamberti, G. Spoto, D. Scarano, C. Paze, M. Salvalaggio, S. Bordiga, A. Zecchina, G. Turnes Palomino, F. DAcapito, *Chem. Phys. Lett.* **1997**, *269*, 500-508.
[7] A. Zecchina, D. Scarano, S. Bordiga, G. Spoto, C. Lamberti, *Adv. Catal.* **2001**, *46*, 265-397.
[8] P. S. Braterman, *Metal Carbonyl Spectra*; Academic Press: London, **1975**.
[9] C. Engemann, J. Hormes, A. Longen, K. H. Dotz, *Chem. Phys.* **1998**, *237*, 471-481.
[10] C. Lamberti, G. Turnes Palomino, S. Bordiga, G. Berlier, F. D'Acapito, A. Zecchina, *Angew. Chem. Int. Ed.* **2000**, *39*, 2138-2141.
[11] C. Prestipino, L. Capello, F. D'Acapito, C. Lamberti, *Phys. Chem. Chem. Phys.* **2005**, *7*, 1743-1746.
[12] A. L. Ankudinov, A. I. Nesvizhskii, J. J. Rehr, *Phys. Rev. B.* **2003**, *67*, 115120.
[13] B. Ravel, M. Newville, *J. Synchrot. Radiat.* **2005**, *12*, 537-541.
[14] A. L. Ankudinov, B. Ravel, J. J. Rehr, S. D. Conradson, *Phys. Rev. B* **1998**, *58*, 7565-7576.
[15] J. Estephane, E. Groppo, A. Damin, J. G. Vitillo, D. Gianolio, C. Lamberti, S. Bordiga, C. Prestipino, S. Nikitenko, E. A. Quadrelli, M. Taoufik, J. M. Basset, A. Zecchina, *J. Phys. Chem. C* **2009**, *113*, 7305-7315.
[16] P. Fornasini, *Introduction to X-ray absorption spectroscopy*, in: Synchrotron Radiation: Fundamentals, Methodologies and Applications; Mobilio, S.; Vlaic, G., Ed.; Italian Physical Society (SIF): Bologna, **2003**; Vol. 82, p. 129-169.
[17] E. A. Stern, *Phys. Rev. B* **1993**, *48*, 9825-9827.